

Research Article

Ultrafast, high modulation depth terahertz modulators based on carbon nanotube thin films



Maria G. Burdanova^{a,*}, Gleb M. Katyba^b, Reza Kashtiban^a, Gennady A. Komandin^b, Edward Butler-Caddle^a, Michael Staniforth^a, Aram A. Mkrtchyan^c, Dmitry V. Krasnikov^c, Yuriy G. Gladush^c, Jeremy Sloan^a, Albert G. Nasibulin^{c,d}, James Lloyd-Hughes^a

^a University of Warwick, Department of Physics, Gibbet Hill Road, Coventry, CV4 7AL, UK

^b Prokhorov General Physics Institute of the Russian Academy of Sciences, Vavilova Str. 38, Moscow, 119991, Russia

^c Skolkovo Institute of Science and Technology, Nobel Str. 3, 121205, Moscow, Russian Federation

^d Aalto University, School of Chemical Engineering, Kemistintie 1, FI-00076, Espoo, Finland

ARTICLE INFO

Article history:

Received 11 September 2020

Received in revised form

14 October 2020

Accepted 1 November 2020

Available online 6 November 2020

Keywords:

Terahertz modulator

Carbon nanotubes

THz-TDS

Ultrafast devices

ABSTRACT

The development of THz technology and communication systems is creating demand for devices that can modulate THz beams rapidly. Here we report the design and characterisation of high-performance, broadband THz modulators based on the photo-induced transparency of carbon nanotube films. Rather than operating in the standard modulation mode, where optical excitation lowers transmission, this new class of modulators exhibits an inverted modulation mode with an enhanced transmission. Under femtosecond pulsed illumination, modulation depths reaching +80% were obtained simultaneously with modulation speeds of 340 GHz. The influence of the film thickness on the insertion loss, modulation speed and modulation depth was explored over a frequency range from 400 GHz to 2.6 THz. The excellent modulation depth and high modulation speed demonstrated the significant potential of carbon nanotube thin films for ultrafast THz modulators.

© 2020 Elsevier Ltd. All rights reserved.

1. Introduction

Increased communications speeds of tens to hundreds of Gbit/s are needed in the near future to enable ultrafast data transfer rates between wireless devices and routers. Spectral windows in the hundreds of GHz range avoid atmospheric water vapour absorption lines [1], offering the possibility of higher carrier frequencies than current GHz technologies. Hence, wireless communications based at 300–400 GHz are developing rapidly due to the potential for high data transfer rates [2–6]. For example, Wang et al. presented a communications link with data transfer at 3 Gbit/s using a carrier frequency of 0.34 THz [6].

In order to actively control beams of THz radiation, for instance using amplitude modulation, it is desirable to obtain a large modulation depth (MD) and a fast modulation speed (MS) at the target frequency. Recently, the development of various THz modulators using either electrical or optical tuning has been reported [7–10]. In electrically-tuned modulators the free-carrier absorption of

injected charges modulates the THz signal, and the transmission bandwidth and MD are limited by factors including the dielectric function, carrier density and mobility. Modulators based on a 2D electron gas (in GaAs/AlGaAs or GaN/AlGaN heterostructures) had a maximum intensity modulation depth of 93 % [11,12], while recent modulators based on monolayer graphene can reach 99 % in reflection at Brewster's angle [9]. However, the MS is typically in the range of kHz–MHz [9,13], limited by the device's resistance and capacitance. This limitation would need to be overcome for application in high-speed wireless communications.

Optical charge injection affords a faster response time, in principle limited by the carrier recombination lifetime [8]. Traditional semiconductors, such as GaAs, Ge and Si, were initially explored for optical THz modulation and benefit from a high MD (up to 100 %) and a low insertion loss [8], but suffer from slow recombination times, typically exceeding 10 ns, that limit the MS. Low-temperature-grown GaAs has faster picosecond recombination times due to its higher defect density, however its lower mobility means it struggles to obtain substantial MD (< 40 %) [14]. Nanomaterials with optically tunable properties have also been studied as active modulation devices. Among them, graphene and transition metal dichalcogenides (TMDs) show attractively fast carrier

* Corresponding author.

E-mail address: m.burdanova@warwick.ac.uk (M.G. Burdanova).

recombination, which can overcome the MS limit of traditional semiconductors [8,15,16], and retain a low insertion loss [17]. However, they still exhibit a weak MD even at high laser fluence. When considering that graphene is an atom-thick material, the achieved MD is quite remarkable, however the overall performance cannot compete with bulk materials.

Recently a novel negative photoconductivity effect, common to 1D and 2D semiconductors and semi-metals, has been actively studied [18–25]. This effect is based on the enhancement of the THz radiation transmitted through a sample after pulsed optical excitation. Studies to date have focussed on understanding the fundamental mechanisms behind this effect, with stimulated THz emission, enhanced carrier-carrier or carrier-optical phonon scattering, carrier heating and trion formation discussed in the literature. However, the possibility of using this optical effect in THz signal modulation has not been discussed to date, in particular due to the low MD achieved in the previous studies (< 20%).

In this work we demonstrate that high-speed THz modulators with a large MD can be created using thin films of ultralong single-walled carbon nanotubes (SWCNTs). A high MD of + 80 % and a MS above 300 GHz were obtained using the strong photoinduced transparency (or negative photoconductivity) of free-standing SWCNT films. The performance of the modulators was explored over the 0.4–2.6 THz frequency range and optimised using thin SWCNT films grown with different thicknesses. The presented effect, based on the enhancement of THz radiation transmitted through a sample after pulsed optical excitation, offers a new approach to manipulate THz waves.

2. Material and methods

2.1. Sample fabrication

SWCNTs were synthesized by an aerosol CVD method based on the thermal decomposition of a ferrocene catalysts precursor in carbon monoxide atmosphere [26]. The aerosol was directed onto nitrocellulose membrane filters to collect films of SWCNTs. The collection time was varied to create films with different thicknesses, which were labelled by their optical transmittance at 550 nm, which varied from 95 % for the thinnest film to 60 % for the thickest film. The films had thicknesses varying from 11 nm to 106 nm. All SWCNT films were synthesized under the same conditions, and consisted of nearly equilibrium composition: one-third metallic and two-third semiconducting CNTs.

The SWCNT films were deposited on circular metallic frames with an internal diameter of 3 cm using a dry transfer technique [26], and the polymer nitrocellulose membrane filter was removed. This created free-standing films where the CNTs were isolated, without a substrate. A wafer of semi-insulating GaAs was used as a readily-available benchmark for comparison.

2.2. Microscopic analysis

Portions of the same films described above were deposited onto copper TEM grids for analysis. The microstructure of the samples was characterised using a doubly corrected JEOL ARM200F TEM equipped with a Schottky gun. Annular dark field STEM (ADF-STEM) analysis was performed at operating voltage of 80 kV. ADF-STEM images were obtained using a JEOL annular field detector with a fine-imaging probe, at a current of approximately 23 pA with a convergence semi-angle of ~21 mrad and a collection angle of 45–180 mrad. ADF-STEM images were acquired as a single scan of $1,024 \times 1,024$ pixels with a dwell time of 20 μ s per pixel.

2.3. Absorption and Raman spectroscopy

Equilibrium absorbance spectroscopy measurements were performed via UV–vis-IR spectrophotometer (PerkinElmer Lambda 1050, 200–2500 nm), Fourier-transform infrared spectroscopy (Bruker Vertex 70 V, 2.5–75 μ m), THz time-domain spectroscopy (75–1500 μ m) [27] and backward-wave oscillator based THz spectroscopy (3000–6000 μ m) [28]. The experimental transmission T was converted to absorbance assuming $A = -\log_{10}T$. Raman spectra were obtained using a confocal microspectrometer (Labram, Jobin-Yvon Horiba) using a 660 nm laser at 0.58 mW power (spectral resolution 1 cm^{-1} and spatial resolution 1.5 μ m).

2.4. Optical pump, THz probe spectroscopy

The pump beam for optical pump, THz probe (OPTP) spectroscopy was created by an optical parametric amplifier (TOPAS), seeded by a 1 kHz, 40 fs, 800 nm pulse (from a Newport Spectra Physics Spitfire ACE) to create pulses with a tunable center wavelength. Here, a pump wavelength of 650 nm was used (above the E_{11} and E_{22} excitonic absorption lines of the CNTs). The probe frequency varied from 0.3 THz to 2.7 THz. As the SWCNTs used have narrow bandgaps any wavelength shorter than 2.5 μ m can be used. Further details of the experimental setup are reported in Refs. [29]. To measure in reflection, a silver-coated prism was placed near the focus of the OPTP spectrometer. The THz beam reflected from one side of the prism, onto the sample, off the second face of the prism and subsequently continued along the initial THz beam axis. The angle of incidence was < 15° from normal incidence.

3. Results

3.1. Optical spectroscopy and electron microscopy

The quality of the samples were evaluated by using transmission electron microscopy (TEM) and absorption, Raman and THz spectroscopy (Fig. 1). The UV–vis-IR absorption properties of the SWCNT films are shown in Fig. 1a. It is clear from the plot that with an increase in the deposition time the optical absorption increases. The SWCNT film absorbance, $A(\lambda)$, at one particular wavelength, λ , is linearly dependent on the film thickness, d , and the absorption coefficient, α , which can be described through the Lambert-Beer law as $A(\lambda) = \alpha(\lambda)d$. The thicknesses of the SWCNT films were 11, 22, 47, 74 and 106 nm respectively [30,31].

In Fig. 1a the strong π -plasmon absorption of the CNTs (at 279 nm) is accompanied by three excitonic absorption bands corresponding to semiconducting (E_{11}^S and E_{22}^S) and metallic (E_{11}^M) SWCNTs at 2300 nm, 1240 nm and 870 nm respectively. By using a Kataura plot, we determined an average diameter of 1.8 nm, consistent with the diameter observed directly in TEM (see below). The range of NT diameters contributes to the broadening of the excitonic bands.

Fig. 1b shows the G and D Raman bands. The high quality (low number of defects) of the samples is evident from the low D mode intensity in comparison with the G band ($I_G/I_D > 100$). A small blueshift of the G band was observed with a decrease in the film thickness. This can be attributed to changes in the amount of oxygen doping per CNT. Thinner films had a lower number of CNTs per bundle (as evidenced by TEM, see below), and hence a greater fraction of CNTs at the surface of the bundles. As samples were stored in air and were not annealed prior to measurements to desorb any oxygen, the outermost CNTs in each bundle were doped. Hence thinner films (smaller bundles) had more doping per CNT.

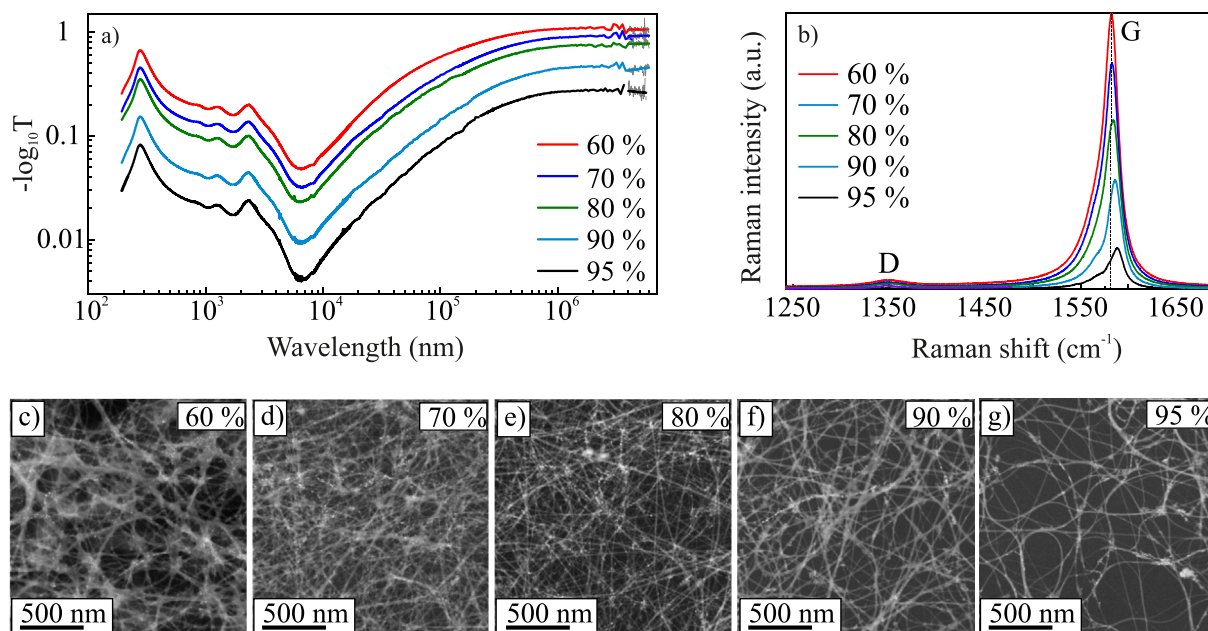


Fig. 1. (a) Absorption and (b) Raman spectra of different SWCNT films. Data are shown for 5 films, labelled by their transmittance at 550 nm as 60 %, 70 %, 80 %, 90 % and 95 %, corresponding to the five different thicknesses 106, 74, 47, 22 and 11 nm respectively. TEM images of SWCNT films with 95 %, 90 %, 80 %, 70 % and 60 % transmittance from the right-hand to the left-hand side. (A colour version of this figure can be viewed online.)

Low magnification TEM images demonstrate the films consisted of high purity, randomly oriented NTs (Fig. 1c–g). In this figure the thickness of the samples increases from the right-hand to the left-hand side. The small nanoparticles on the SWCNT film surface are Fe catalysts. All samples show a percolated NT network with only a small number of individual SWCNTs. The far-right column of Fig. 1 shows that the SWCNT bundles in the thinnest film have a narrower diameter. The average individual SWCNT diameter was found to be 1.8 nm with an average length above 10 μm . In the thinnest sample around 90 % of the SWCNTs were grouped into bundles, due to the strong van der Waals interactions between the individual CNTs, with around 10 % individualised CNTs.

Using multiple TEM images we extracted information about the bundle diameter and the distance between interbundle contacts. With an increase in film thickness, the bundle size grew from 17.9 nm to 30.3 nm, which can be understood as follows. A longer deposition time caused an increase in bundle size, due to the van der Waals interactions between CNTs that are already deposited on the polymer membrane, and the NTs that are newly arriving. The extra NTs shortened the mean spacing between bundle-to-bundle contacts from 88 nm to 21 nm for the thinnest and thickest samples.

3.2. THz conductance and shielding effectiveness

As the wavelength increases, the optical transmission decreased (absorbance increased, Fig. 1a) monotonically through the infrared towards the THz range as a result of the conductivity associated with delocalized carriers (described by the Drude model) and axial plasmon motion [32]. When SWCNTs form an extended network, a strong Drude contribution is expected to be seen. In the frequency range from 70 GHz to 300 GHz range, the effective conductance ($\sigma \times d$) of the films is higher for the thicker films varying between 2.5 mS (thinnest film) and 16 mS (thickest film), as determined from transmission measurements using BWOs and THz-TDS.

A higher conductance results in a higher shielding effectiveness (SE), which is the electric field insertion loss in free space for a plane

wave at normal incidence and is defined by $SE = 20\log_{10}(|E_R|/|E_S|) = -20\log_{10}|t|$, where E_S and E_R are the field strength measured with and without sample respectively and $t = E_S/E_R$. The SE can also be calculated from the optical density (absorbance $A = -\log_{10}|t|^2$) as $SE = 10A$. The SE can be tuned by the sample thickness, and varied from 10.5 dB (~ 0.11 dB/nm) for the thickest sample to 2.7 dB (~ 0.3 dB/nm) for the thinnest sample. A higher shielding effectiveness (higher insertion loss) is beneficial for electromagnetic screening applications [33], but is not desirable for standard ultrafast optical modulators operating in photoinduced absorption mode. However, for the inverted operation mode used here, based on photoinduced transparency, a greater SE in equilibrium yields an increased modulation depth, as discussed in the following section.

3.3. Ultrafast optical modulation

The THz transmission of a medium is a function of its conductivity [34]. Therefore, the THz transmission can be modulated by changing a material's conductivity using optical excitation. The MD is a key parameter and can be defined by $MD = \Delta E/E = (E_{ON} - E_{OFF})/E_{OFF}$, where E_{OFF} and E_{ON} are THz electric field strength in equilibrium and under photoexcitation respectively. In traditional THz modulators based on traditional semiconductors (e.g. III-V semiconductors) the photoinduced free carriers attenuate the THz radiation, reducing the transmitted field strength ($E_{ON} < E_{OFF}$) and giving “negative” THz modulation ($MD < 0$). Results using semi-insulating GaAs as such a modulator are shown in Fig. 2a, where the average THz transmission (dashed blue line) relative to the incident amplitude is plotted as a function of time after a 650 nm excitation pulse (fluence 210 $\mu\text{J}/\text{cm}^2$). Before the pump arrives, the transmission is high (low insertion loss, $SE = 3.34$ dB). When pumped E_{ON} lowers rapidly as a result of the strong absorption of GaAs and its relatively good electron mobility. This yields a large MD of -83% , but the slow carrier recombination time (> 1 ns) leads to a poor MS.

In contrast to the negative MD of GaAs, the SWCNT thin films showed an inverted operation mode, where optical excitation

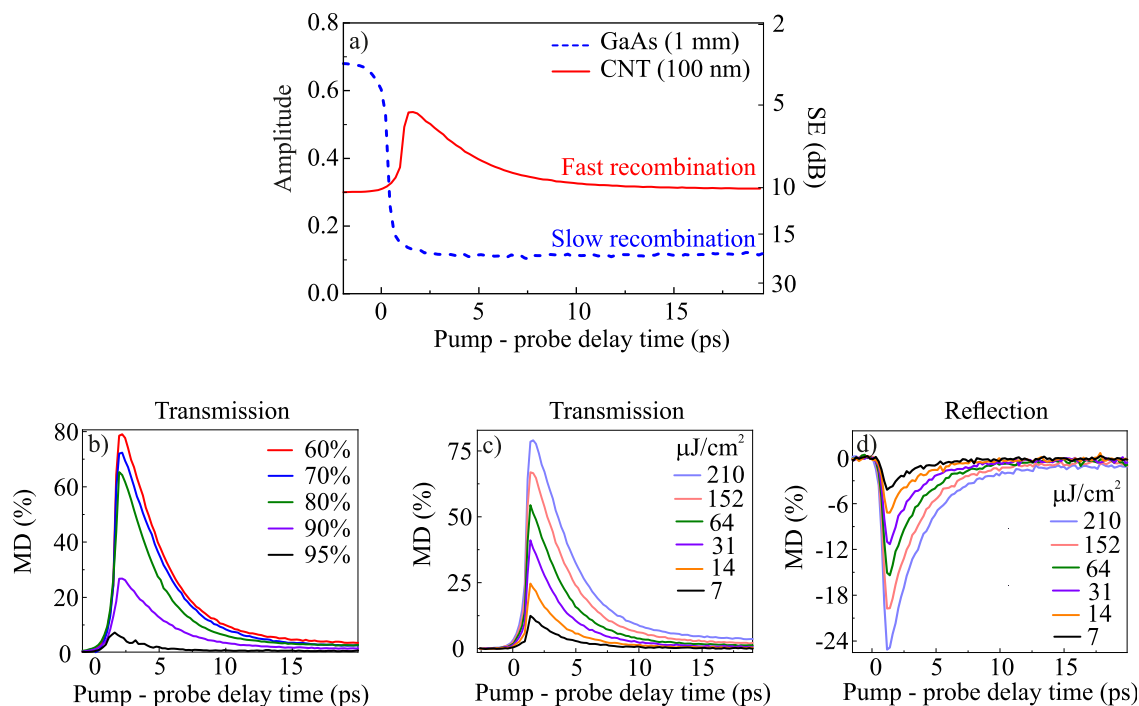


Fig. 2. (a) The transmission of GaAs- and SWCNT-based modulators under 650 nm excitation with a fluence of $210 \mu\text{J}/\text{cm}^2$. (b) Modulation depth in transmission, as a function of pump-probe delay time, for samples with different thicknesses under the same pump conditions as in (a). (c) In transmission mode MD for 60% sample at fluences varying from 7 to $210 \mu\text{J}/\text{cm}^2$. (d) 60% sample in the reflection geometry for the same fluences as in (c). (A colour version of this figure can be viewed online.)

triggered an increase in transmission, and a positive MD. For the thickest SWCNT film, a large positive MD of +80% was obtained under the same excitation conditions as for GaAs (solid red line in Fig. 2a), and with a recovery on picosecond timescales. The physical origin of this photoinduced transparency, a reduction in the overall conductivity of the film, is still under debate. While some studies assigned it to trion formation that lowers the total carrier density and increases the average effective mass, other studies attributed it to heat-induced changes [22,24,25]. The modulator reached its highest MD within a few ps, before reverting back to its equilibrium level after around 15 ps. We also checked a sample deposited on a quartz substrate which had a MD and MS comparable to its free-standing counterpart, but has the added benefit of being mechanically robust.

The modulation speed is another important parameter for the use of THz modulators in high-speed applications. Here we defined the maximum operation frequency as $MS = 1/\tau$ using exponential fits to $\Delta E/E$ with lifetime τ . This yielded $MS = 300 \text{ GHz}$ (for $\tau = 3.3 \text{ ps}$), significantly faster than for the GaAs modulator, which had $MS < 0.5 \text{ GHz}$ ($\tau > 2 \text{ ns}$). Silicon-based modulators have even longer recombination times (microseconds to milliseconds) and consequently have lower MS [35].

To further explore this new class of ultrafast THz modulators we measured the MD as a function of film thickness, which varied the optical density in the visible and THz ranges simultaneously (Fig. 1a). With an increase in thickness the MD increased monotonically from about 10% to 80% (Fig. 2b). The thicker films absorbed a greater fraction of the incident pump beam, yielding a larger MD. Simultaneously, the insertion loss in equilibrium increased for thicker films, lowering the transmission in the “off” state, before photoexcitation. While a higher insertion loss can be detrimental for the performance of normal modulators ($MD < 0$), it has less consequences for the present inverted modulators ($MD > 0$): as long as the photoinduced transparency is strong, the “on” state transmission is high, which results in a high MD.

Precise control of the MD can be achieved by tuning the modulation beam’s fluence. Below $40 \mu\text{J}/\text{cm}^2$ a linear change of the MD with fluence was observed, while at higher fluence the MD was saturated (Fig. 2c). Increasing the fluence over $210 \mu\text{J}/\text{cm}^2$ damaged the samples. Even at $7 \mu\text{J}/\text{cm}^2$ the MD was 12%, which is comparable to literature results based on graphene and MoS_2 at significantly higher fluence (see Discussion).

For optically pumped THz modulators, the fraction of the pump beam absorbed is a relevant figure of merit, and it is informative to compare the performance of the SWCNTs to that of GaAs. For the GaAs single crystal at normal incidence, around 34% of the pump beam was reflected, while the remaining 66% was absorbed in a penetration depth of 200 nm [36]. For the thickest SWCNT film ($\sim 90 \text{ nm}$) around 40% of the pump was absorbed in a shorter distance (90 nm) than the penetration depth of GaAs (200 nm). This highlights the excellent optical absorption of the CNT films.

Fig. 2d shows the operation of the same modulator but measured in reflection. A reduction in the amplitude of reflected THz beam was observed under the optical excitation, similar to the report by Tasolamprou et al. for graphene [37]. In equilibrium, the reflected THz signal is high (the high sheet conductivity of the film creates a high reflectivity - higher than 85% at near normal incidence), then after photoexcitation more THz is transmitted through the film (less is reflected). Hence in the reflection geometry the SWCNTs act as a modulator with a negative MD (normal operation, like positive photoconductors in transmission). A 27% MD with a MS of 400 GHz were achieved at a fluence of $210 \mu\text{J}/\text{cm}^2$ which are significantly higher than previously reported values [18]. The MD was smaller than the MD in transmission at the same incident laser power, partially because the pump beam was at an oblique angle rather than at normal incidence as was used for the transmission experiments.

The MD discussed above, was the modulation of the electric field at the peak of the THz pulse in the time-domain, which

corresponds to a frequency-averaged response. However the frequency-dependent performance of the SWCNT modulator is also important. In Fig. 3 the frequency-dependent MD is reported at a time delay of 3 ps after laser irradiation, for the thickest SWCNT film, and for different fluences. As the MD is a complex number in the frequency domain, both $|MD|$ and $\arg(MD)$ are reported. A substantial amplitude modulation can be observed for all fluences and is most pronounced at lower frequencies (as the equilibrium conductivity increases at lower frequency, and is suppressed on photoexcitation [24]). Given the finite THz pulse duration (~ 0.5 ps) and the rapid dynamic change in THz conductivity, 3 ps was chosen rather than closer to zero delay, and hence the average $|MD(\omega)|$ is lower than the peak MD in the time-domain at zero delay (Fig. 2b). The phase of the modulation depth, $\arg(MD)$, was relatively flat at each fluence, and increased from 0.01π to 0.11π over the range of fluences (Fig. 3b). As the SWCNTs act as a relatively broadband modulator, their phase change at a particular frequency is lower than reported in some metamaterial-based phase modulators. For example, phase shifters based on vanadium dioxide nanostructures and metasurfaces obtained a phase shift of $\pm 0.4\pi$ [38,39]. Future studies may combine SWCNTs with metasurfaces in order to obtain modulators with narrower resonances, and larger phase changes, which are desired for some applications.

4. Discussion

The energy modulation factor (EMF), η , is a metric that allows the performance of a modulator to be assessed, and is defined by

$$\eta = \frac{\int |E_{\text{OFF}}(\omega)|^2 d\omega - \int |E_{\text{ON}}(\omega)|^2 d\omega}{\int |E_{\text{OFF}}(\omega)|^2 d\omega}$$

where the integration is over the frequency range of the THz pulse (0.37–2.6 THz). This approach has been widely used to characterise modulators based on graphene [40], metamaterials [41], organometal halide perovskites [42], polymer-based organic films [43] and organic-inorganic hybrid structures [44]. For normal modulators (based on photoinduced absorption) η is positive, as the energy of the transmitted beam is lower under photoexcitation. In contrast, η is negative for the SWCNT films: for the thickest SWCNT film the EMF varied from $\eta = -0.1$ to $\eta = -0.99$ with an increase in fluence from 7 to $210 \mu\text{J}/\text{cm}^2$. The negative value indicates an increase of the

transmission under optical photoexcitation. The obtained absolute value, $|\eta| = 0.99$, is similar to values reported for optically-excited polymer/silicon modulators for a similar frequency range [40], which have $MS \sim 1$ kHz. The EMF obtained here for GaAs under the same experimental conditions varied between $\eta = +0.09$ and $\eta = +0.95$ over the same fluence range, similar to reports in Refs. [45].

To facilitate further comparison with other material systems, we collated representative results for different semiconductor (nano) materials, and present this summary in Fig. 4a and b for inverted ($\Delta E/E > 0$) and traditional ($\Delta E/E < 0$) operation modes respectively. The results show that for all SWCNT film thicknesses the MD values are higher than what has been reported for graphene [18–20,46] and their MS values are similar to graphene's being in the range 300–460 GHz. Graphene's relatively weak optical absorption leads to the lower MD in comparison to the SWCNT films. On reducing the thickness of the SWCNT films the MD lowered to values similar to graphene, while the MS increased (blue points in Fig. 4a). In contrast to SWCNTs, the photoinduced change in transmission in stacked graphene and graphite is relatively independent of the thickness [47].

Modulators based on photoinduced THz transparency ($MD > 0$) in atomically-thin TMDs such as MoS_2 have been reported, however their MD is lower ($\sim 5\%$) than in the present case even at a comparable fluence [21,23]. It was reported that the same materials can also show normal photoconductivity ($MD = \Delta E/E < 0$) after annealing [18,23,48]. However, the MD and MS are still lower than for the present CNTs (Fig. 4b). CdTe nanowires and GaAs-based nanostructures can have reasonable MD or MS but not both simultaneously [49–54]. Among all the materials surveyed, the thin films of long SWCNTs reported here demonstrate uniquely high MD combined with fast MS.

For applications in THz communications, the high MS obtained would enable faster data transfer rates via amplitude modulation. Such SWCNT thin films can therefore be used as a high speed visible-to-THz optical interconnect that works at any wavelength where the CNTs absorb (up to $2.5 \mu\text{m}$ in the present case). Importantly, however, similar SWCNT films can be grown with excitonic absorption resonances better matched to the telecommunications band around $1.5 \mu\text{m}$ [55].

The high MD and large insertion loss (in equilibrium) may allow these SWCNT films to be used as an ultrafast shutter that allows the transmission of a very short signal. The speed of such an optical shutter far exceeds that of mechanical or electrical shutters. This

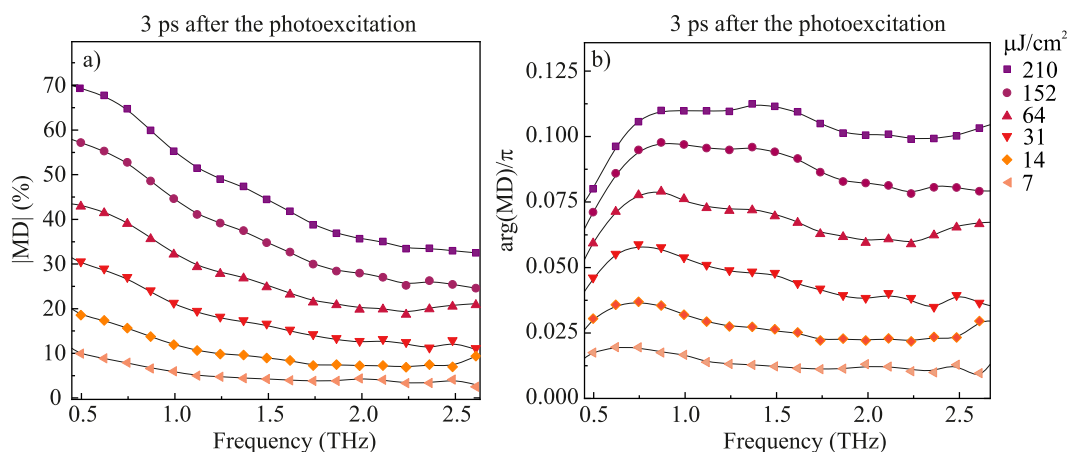


Fig. 3. Frequency dependence of modulation depth at 3 ps after photoexcitation. The frequency dependent modulation depth (a) and the change of phase (b) of the 60-nm-sample at 650 nm under fluences varying between 7 and $210 \mu\text{J}/\text{cm}^2$. (A colour version of this figure can be viewed online.)

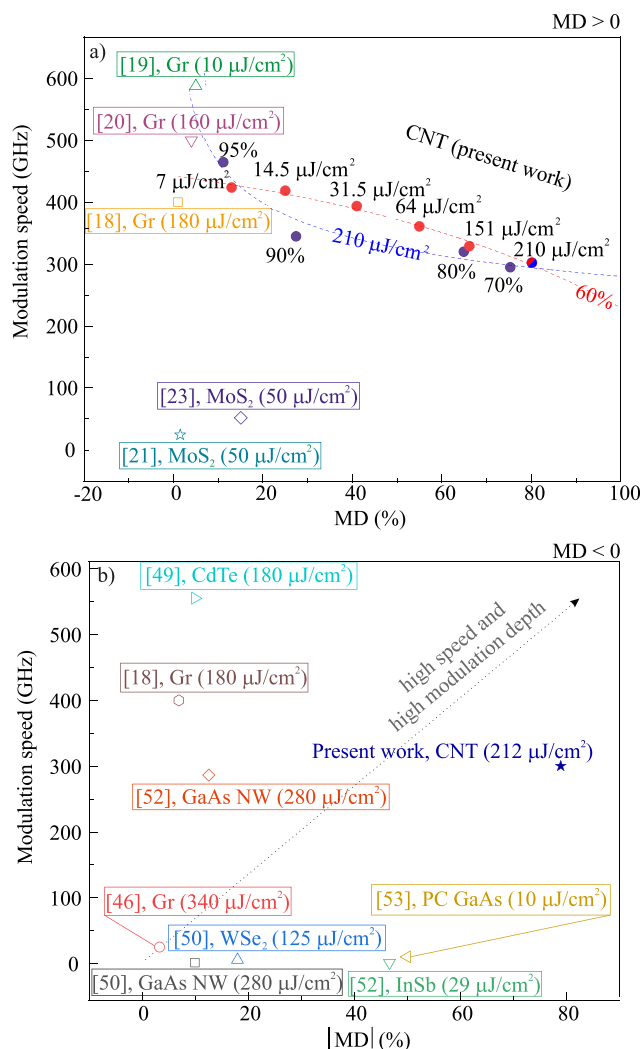


Fig. 4. Performance of optical THz modulators based on different nanomaterials. The frequency-averaged MD (at the peak of the time-domain THz pulse) at zero pump-probe delay was used for this comparison. (a) Modulators based on positive $\Delta E/E > 0$. Open markers show literature values; filled red circles are the 60% SWCNT film at different pump fluences for 650 nm excitation, and the filled blue circles are at the same pump wavelength but for different samples at 210 $\mu\text{J}/\text{cm}^2$ only. (b) Modulators based on $\Delta E/E < 0$, from literature (open markers). Gr stands for graphene, NW for nanowires, and PC for photonic crystal. For comparison, a result is also shown for the present modulator with $\Delta E/E > 0$ (filled blue star), for the 60% sample excited at 650 nm with 212 $\mu\text{J}/\text{cm}^2$. (A colour version of this figure can be viewed online.)

may have applications, for instance, in pulse slicers or pulse pickers that create short THz pulses from a bright CW (or relatively long pulse) THz beam such as a free electron laser, using the photoinduced transparency of the SWCNT film to define a short pulse.

We now describe some design considerations that could further improve this new class of THz modulators. To increase the MD, higher fluences cannot be used as higher powers than reported here damaged the free-standing SWCNT films. There is room, however, to make more efficient use of the pump photons by using a shorter excitation wavelength, where the absorbance of the SWCNT films is higher. Free-standing SWCNT films are very fragile, but can be transferred to a substrate with low THz absorption (e.g. crystalline quartz), providing a more mechanically robust modulator and without compromising the MS or MD. The high MS of the modulator benefits from the short (1 ps) lifetime of carriers in SWCNT thin films. Previous work has shown the lifetime can be shortened by electrical gating or doping [24], although the lower

mobility of such modified SWCNT films may be detrimental to the MD.

5. Conclusions

A novel, ultrafast THz modulator based on photoinduced transparency was presented. We showed experimentally that the photoinduced THz transparency of as-grown, long SWCNTs can be used for the optical modulation of THz waves at modulation speeds of more than 300 GHz and with modulation depths up to +80%. We supplemented ultrafast THz spectroscopy measurements with Raman, UV–vis-IR spectroscopy and TEM microscopy to evaluate the quality of the SWCNT network in addition to the optoelectronic properties.

CRediT authorship contribution statement

Maria G. Burdanova: Methodology, Data curation, Writing - original draft, Investigation, Formal analysis. **Gleb M. Katyba:** Investigation. **Reza Kashtiban:** Investigation, Writing - review & editing. **Gennady A. Komandin:** Investigation. **Edward Butler-Caddle:** Investigation. **Michael Staniforth:** Investigation, Writing - review & editing. **Aram A. Mkrtchyan:** Resources. **Dmitry V. Krasnikov:** Resources. **Yuriy G. Gladush:** Resources, Writing - review & editing. **Jeremy Sloan:** Funding acquisition, Supervision. **Albert G. Nasibulin:** Funding acquisition, Supervision, Writing - review & editing. **James Lloyd-Hughes:** Conceptualization, Methodology, Supervision, Writing - original draft, Writing - review & editing, Project administration, Funding acquisition.

Declaration of competing interest

The authors declare that they have no known competing financial interests or personal relationships that could have appeared to influence the work reported in this paper.

Acknowledgements

MGB acknowledges support from the Global Education Program (Russia) for a PhD scholarship. The UK authors acknowledge the EPSRC (UK) for funding under grant EP/N010825/1. AAM and DVK acknowledge the Russian Science Foundation project No. 20-73-10256 (synthesis of carbon nanotubes). The reported study was funded by RFBR according to the research project No. 20-32-90233.

References

- [1] D.M. Slocum, E.J. Slingerland, R.H. Giles, T.M. Goyette, Atmospheric absorption of terahertz radiation and water vapor continuum effects, *J. Quant. Spectrosc. Radiat. Transf.* 127 (2013) 49–63, <https://doi.org/10.1016/j.jqsrt.2013.04.022>.
- [2] T. Nagatsuma, T. Takada, H. Song, K. Ajito, N. Kukutsu, Y. Kado, Millimeter- and thz-wave photonics towards 100-Gbit/s wireless transmission, in: 2010 23rd Annual Meeting of the IEEE Photonics Society, 2010, pp. 385–386, <https://doi.org/10.1109/PHOTONICS.2010.5698921>.
- [3] H. Song, K. Ajito, A. Wakatsuki, Y. Muramoto, N. Kukutsu, Y. Kado, T. Nagatsuma, Terahertz wireless communication link at 300 GHz, in: 2010 IEEE International Topical Meeting on Microwave Photonics, 2010, pp. 42–45, <https://doi.org/10.1109/MWP.2010.5664230>.
- [4] S. Koenig, F. Boes, D. Lopez-Diaz, J. Antes, R. Henneberger, R. Schmogrow, D. Hillerkuss, R. Palmer, T. Zwick, C. Koos, W. Freude, O. Ambacher, I. Kallfass, J. Leuthold, 100 gbit/s wireless link with mm-wave photonics, in: 2013 Optical Fiber Communication Conference and Exposition and the National Fiber Optic Engineers Conference (OFC/NFOEC), 2013, pp. 1–3, <https://doi.org/10.1364/OFC.2013.PDP5B.4>.
- [5] T. Nagatsuma, 300-GHz -band wireless communications with high-power photonic sources, in: 2014 XXXIth URSI General Assembly and Scientific Symposium (URSI GASS), 2014, pp. 1–4, <https://doi.org/10.1109/URSIGASS.2014.6929496>.
- [6] C. Wang, B. Lu, C. Lin, Q. Chen, L. Miao, X. Deng, J. Zhang, 0.34-THz wireless link based on high-order modulation for future wireless local area network

- applications, *IEEE Transactions on Terahertz Science and Technology* 4 (1) (2014) 75–85, <https://doi.org/10.1109/THZ.2013.2293119>.
- [7] D.K. Kim, D.S. Citrin, Frequency and amplitude modulation in terahertz-sideband generation in quantum wells, *Appl. Phys. Lett.* 94 (2) (2009), 021105, <https://doi.org/10.1063/1.3068494>.
- [8] M. Rahm, J.-S. Li, W.J. Padilla, Thz wave modulators: a brief review on different modulation techniques, *J. Infrared, Millim. Terahertz Waves* 34 (1) (2013) 1–27, <https://doi.org/10.1007/s10762-012-9946-2>.
- [9] Z. Chen, X. Chen, L. Tao, K. Chen, M. Long, X. Liu, K. Yan, R.I. Stantchev, E. Pickwell-MacPherson, J.-B. Xu, Graphene controlled Brewster angle device for ultra broadband terahertz modulation, *Nat. Commun.* 9 (1) (2018) 4909, <https://doi.org/10.1038/s41467-018-07367-8>. URL: <http://www.nature.com/articles/s41467-018-07367-8>.
- [10] L. Wang, Y. Zhang, X. Guo, T. Chen, H. Liang, X. Hao, X. Hou, W. Kou, Y. Zhao, T. Zhou, S. Liang, Z. Yang, A review of THz modulators with dynamic tunable metasurfaces, *Nanomaterials* 9 (7) (2019) 965, <https://doi.org/10.3390/nano9070965>.
- [11] R. Kersting, G. Strasser, K. Unterrainer, Terahertz phase modulator, *Electron. Lett.* 36 (13) (2000) 1156–1158.
- [12] T. Kleine-Ostmann, P. Dawson, K. Pierz, G. Hein, M. Koch, Room-temperature operation of an electrically driven terahertz modulator, *Appl. Phys. Lett.* 84 (18) (2004) 3555–3557, <https://doi.org/10.1063/1.1723689>.
- [13] B. Sensale-Rodriguez, R. Yan, S. Rafique, M. Zhu, W. Li, X. Liang, D. Gundlach, V. Protasenko, M. Kelly, D. Jena, L. Liu, H.G. Xing, Extraordinary control of terahertz beam reflectance in graphene electro-absorption modulators, *Nano Lett.* 12 (9) (2012) 4518–4522, <https://doi.org/10.1021/nl3016329>.
- [14] M.C. Beard, G.M. Turner, C.A. Schmuttenmaer, Subpicosecond carrier dynamics in low-temperature grown GaAs as measured by time-resolved terahertz spectroscopy, *J. Appl. Phys.* 90 (12) (2001) 5915–5923, <https://doi.org/10.1063/1.1416140>.
- [15] P. Weis, J.L. Garcia-Pomar, M. Hanah, B. Reinhard, A. Brodyanski, M. Rahm, Spectrally wide-band terahertz wave modulator based on optically tuned graphene, *ACS Nano* 6 (10) (2012) 9118–9124, <https://doi.org/10.1021/nn303392s>, pMID: 22992128.
- [16] D.-S. Yang, T. Jiang, X.-A. Cheng, Optically controlled terahertz modulator by liquid-exfoliated multilayer WS₂ nanosheets, *Optic Express* 25 (14) (2017) 16364–16377, <https://doi.org/10.1364/OE.25.016364>.
- [17] M. Liu, X. Yin, E. Ulin-Avila, B. Geng, T. Zentgraf, L. Ju, F. Wang, X. Zhang, A graphene-based broadband optical modulator, *Nature* 474 (7349) (2011) 64–67, <https://doi.org/10.1038/nature10067>.
- [18] C.J. Docherty, C.T. Lin, H.J. Joyce, R.J. Nicholas, L.M. Herz, L.J. Li, M.B. Johnston, Extreme sensitivity of graphene photoconductivity to environmental gases, *Nat. Commun.* 3 (1228) (2012) 1–6, <https://doi.org/10.1038/ncomms2235>.
- [19] A.J. Frenzel, C.H. Lui, W. Fang, N.L. Nair, P.K. Herring, P. Jarillo-Herrero, J. Kong, N. Gedik, Observation of suppressed terahertz absorption in photoexcited graphene, *Appl. Phys. Lett.* 102 (11) (2013) 113111, <https://doi.org/10.1063/1.4795858>.
- [20] G. Jnawali, Y. Rao, H. Yan, T.F. Heinz, Observation of a transient decrease in terahertz conductivity of single-layer graphene induced by ultrafast optical excitation, *Nano Lett.* 13 (2) (2013) 524–530, <https://doi.org/10.1021/nl303988q>.
- [21] C.H. Lui, A.J. Frenzel, D.V. Pilon, Y.-H. Lee, X. Ling, G.M. Akselrod, J. Kong, N. Gedik, Trion-induced negative photoconductivity in monolayer MoS₂, *Phys. Rev. Lett.* 113 (2014) 166801, <https://doi.org/10.1103/PhysRevLett.113.166801>.
- [22] P. Karlsen, M.V. Shuba, P.P. Kuzhir, A.G. Nasibulin, P. Lamberti, E. Hendry, Sign inversion in the terahertz photoconductivity of single-walled carbon nanotube films, *Phys. Rev. B* 98 (2018) 241404, <https://doi.org/10.1103/PhysRevB.98.241404>.
- [23] X. Xing, L. Zhao, Z. Zhang, X. Lin, Y. Yu, Z. Jin, W. Liu, W. Zhang, G. Ma, The modulation of terahertz photoconductivity in CVD-grown n-doped monolayer W-MoS₂ with gas adsorption, *J. Phys. Condens. Matter* 31 (24) (2019) 245001, <https://doi.org/10.1088/1361-648x/ab0f0a>.
- [24] M.G. Burdanova, A.P. Tsapenko, D.A. Satco, R. Kashtiban, C.D.W. Mosley, M. Monti, M. Staniforth, J. Sloan, Y.G. Gladush, A.G. Nasibulin, J. Lloyd-Hughes, Giant negative terahertz photoconductivity in controllably doped carbon nanotube networks, *ACS Photonics* 6 (4) (2019) 1058–1066, <https://doi.org/10.1021/acsp Photonics.9b00138>.
- [25] M.G. Burdanova, R.J. Kashtiban, Y. Zheng, R. Xiang, S. Chiashi, J.M. Woolley, M. Staniforth, E. Sakamoto-Rablah, X. Xie, M. Broome, J. Sloan, A. Anisimov, E.I. Kauppinen, S. Maruyama, J. Lloyd-Hughes, Ultrafast optoelectronic processes in 1D radial van der Waals heterostructures: carbon, boron nitride, and MoS₂ nanotubes with coexisting excitons and highly mobile charges, *Nano Lett.* 20 (5) (2020) 3560–3567, <https://doi.org/10.1021/acs.nanolett.0c00504>. URL: <https://pubs.acs.org/doi/10.1021/acs.nanolett.0c00504>.
- [26] A.G. Nasibulin, A. Moisala, D.P. Brown, H. Jiang, E. Kauppinen, A novel aerosol method for single walled carbon nanotube synthesis, *Chem. Phys. Lett.* 402 (1–3) (2005) 227–232, <https://doi.org/10.1016/j.cplett.2004.12.040>.
- [27] C. D. W. Mosley, M. Failla, D. Prabhakaran, J. Lloyd-Hughes, Terahertz spectroscopy of anisotropic materials using beams with rotatable polarization, *Sci. Rep.* 7 (1) (2019) 10.1038/s41598-017-12568-0. URL: <https://doi.org/10.1038/s41598-017-12568-0>.
- [28] G.A. Komandin, S.V. Chuchupal, S.P. Lebedev, Y.G. Goncharov, A.F. Korolev, O.E. Porodnikov, I.E. Spektor, A.A. Volkov, BWO generators for terahertz dielectric measurements, *IEEE Transactions on Terahertz Science and Technology* 3 (4) (2013) 440–444, <https://doi.org/10.1109/THZ.2013.2255914>.
- [29] M. Monti, S.X. Tao, M. Staniforth, A. Crocker, E. Griffin, A. Wijesekara, R.A. Hutton, J. Lloyd-Hughes, Efficient intraband hot carrier relaxation in the perovskite semiconductor Cs_{0.1-x}Rb_{0.9-x}Sn_{0.3} mediated by strong electron-phonon coupling, *J. Phys. Chem. C* 122 (36) (2018) 20669–20675, <https://doi.org/10.1021/acs.jpcc.8b07792>. URL: <http://pubs.acs.org/doi/10.1021/acs.jpcc.8b07792>.
- [30] G.A. Ermolaev, A.P. Tsapenko, V.S. Volkov, A.S. Anisimov, Y.G. Gladush, A.G. Nasibulin, Express determination of thickness and dielectric function of single-walled carbon nanotube films, *Appl. Phys. Lett.* 116 (23) (2020) 231103, <https://doi.org/10.1063/5.0012933>, arXiv:.
- [31] G. Drozdzov, I. Ostanin, H. Xu, Y. Wang, T. Dumitrica, A. Grebenko, A.P. Tsapenko, Y. Gladush, G. Ermolaev, V.S. Volkov, S. Eibl, U. Rade, A.G. Nasibulin, Densification of Single-Walled Carbon Nanotube Films: Mesoscopic Distinct Element Method Simulations and Experimental Validation, 2020 arXiv:2008.13046.
- [32] Q. Zhang, E.H. Haroz, Z. Jin, L. Ren, X. Wang, R.S. Arvidson, A. Lattge, J. Kono, Plasmonic nature of the terahertz conductivity peak in single-wall carbon nanotubes, *Nano Lett.* 13 (12) (2013) 5991–5996, <https://doi.org/10.1021/nl403175g>, pMID: 24224898, arXiv:.
- [33] M.V. Shuba, D.I. Yuko, P.P. Kuzhir, S.A. Maksimenko, M.A. Kanygin, A.V. Okotrub, R. Tenne, P. Lambin, How effectively do carbon nanotube inclusions contribute to the electromagnetic performance of a composite material? estimation criteria from microwave and terahertz measurements, *Carbon* 129 (2018) 688–694, <https://doi.org/10.1016/j.carbon.2017.12.067>.
- [34] J. Lloyd-Hughes, T.-I. Jeon, A review of the terahertz conductivity of bulk and nano-materials, *J. Infrared, Millim. Terahertz Waves* 33 (9) (2012) 871, <https://doi.org/10.1007/s10762-012-9905-y>. URL: <http://www.springerlink.com/index/10.1007/s10762-012-9905-y>.
- [35] R. Ulbricht, R. Kurstjens, M. Bonn, Assessing charge carrier trapping in silicon nanowires using picosecond conductivity measurements, *Nano Lett.* 12 (7) (2012) 3821–3827, <https://doi.org/10.1021/nl3017835>.
- [36] E.D. Palik (Ed.), *Handbook of Optical Constants of Solids*, Elsevier, 1985, <https://doi.org/10.1016/c2009-0-20920-2>.
- [37] A.C. Tasolamprou, A.D. Koulouklidis, C. Daskalaki, C.P. Mavidis, G. Kenanakis, G. Deligeorgis, Z. Viskadourakis, P. Kuzhir, S. Tzortzakakis, M. Kafesaki, E.N. Economou, C.M. Soukoulis, Experimental demonstration of ultrafast THz modulation in a graphene-based thin film absorber through negative photo-induced conductivity, *ACS Photonics* 6 (3) (2019) 720–727, <https://doi.org/10.1021/acsp Photonics.8b01595>.
- [38] Y. Zhao, Y. Zhang, Q. Shi, S. Liang, W. Huang, W. Kou, Z. Yang, Dynamic photoinduced controlling of the large phase shift of terahertz waves via vanadium dioxide coupling nanostructures, *ACS Photonics* 5 (8) (2018) 3040–3050, <https://doi.org/10.1021/acsp Photonics.8b00276>.
- [39] Y. Zhang, Y. Zhao, S. Liang, B. Zhang, L. Wang, T. Zhou, W. Kou, F. Lan, H. Zeng, J. Han, Z. Feng, Q. Chen, P. Mazumder, Z. Yang, Large phase modulation of THz wave via an enhanced resonant active hemt metasurface, *Nanophotonics* 8 (1) (2018) 153–170, <https://doi.org/10.1515/nanoph-2018-0116>.
- [40] G. Wang, B. Zhang, H. Ji, X. Liu, T. He, L. Lv, Y. Hou, J. Shen, Monolayer graphene based organic optical terahertz modulator, *Appl. Phys. Lett.* 110 (2) (2017), 023301, <https://doi.org/10.1063/1.4973816>.
- [41] T. Matsui, R. Takagi, K. Takano, M. Hangyo, Mechanism of optical terahertz-transmission modulation in an organic/inorganic semiconductor interface and its application to active metamaterials, *Opt. Lett.* 38 (22) (2013) 4632–4635, <https://doi.org/10.1364/OL.38.004632>.
- [42] X. Zhang, X.F. Qiao, W. Shi, J.B. Wu, D.S. Jiang, P. Tan, Phonon and Raman Scattering of Two-Dimensional Transition Metal Dichalcogenides from Monolayer, Multilayer to Bulk Material, 2015, <https://doi.org/10.1039/c4cs00282b>.
- [43] T. He, B. Zhang, G.-C. Wang, M.-D. Zang, Y.-B. Hou, J.-L. Shen, High efficiency THz-wave modulators based on conjugated polymer-based organic films, *J. Phys. Appl. Phys.* 49 (7) (2016), 075111, <https://doi.org/10.1088/0022-3727/49/7/075111>.
- [44] H. Keun Yoo, S.-G. Lee, C. Kang, C.-S. Kee, J. Wook Lee, Terahertz modulation on angle-dependent photoexcitation in organic-inorganic hybrid structures, *Appl. Phys. Lett.* 103 (15) (2013) 151116, <https://doi.org/10.1063/1.4825170>.
- [45] A.S. Kurdyubov, A.V. Trifonov, I.Y. Gerlovin, I.V. Ignatiev, A.V. Kavokin, Impurity-induced modulation of terahertz waves in optically excited GaAs, *AlP Adv.* 7 (11) (2017) 115222, <https://doi.org/10.1063/1.4995358>.
- [46] S. Kar, D.R. Mohapatra, A.K. Sood, Tunable terahertz photoconductivity of hydrogen functionalized graphene using optical pump-terahertz probe spectroscopy, *Nanoscale* 10 (2018) 14321–14330, <https://doi.org/10.1039/C8NR04154G>.
- [47] H. Choi, F. Borondics, D.A. Siegel, S.Y. Zhou, M.C. Martin, A. Lanzara, R.A. Kaindl, Broadband electromagnetic response and ultrafast dynamics of few-layer epitaxial graphene, *Appl. Phys. Lett.* 94 (17) (2009) 172102, <https://doi.org/10.1063/1.3122348>.
- [48] S. Kar, Y. Su, R.R. Nair, A.K. Sood, Probing photoexcited carriers in a few-layer MoS₂ laminate by time-resolved optical pump-terahertz probe spectroscopy, *ACS Nano* 9 (12) (2015) 12004–12010, <https://doi.org/10.1021/acsnano.5b04804>, pMID: 26516987.
- [49] W. Zhang, J. Guo, P. Suo, L. Lv, J. Liu, X. Lin, Z. Jin, W. Liu, G. Ma, Optically controlled ultrafast terahertz switching in a CdTe nanostructure thin film, *Appl. Opt.* 58 (30) (2019) 8200–8206, <https://doi.org/10.1364/AO.58.008200>.

- [50] H.J. Joyce, J.L. Boland, C.L. Davies, S. Baig, M. Johnston, A review of the electrical properties of semiconductor nanowires: insights gained from terahertz conductivity spectroscopy, *Semicond. Sci. Technol.* 31 (10) (2016) 103003, <https://doi.org/10.1088/0268-1242/31/10/103003>.
- [51] P. Gopalan, A. Chanana, S. Krishnamoorthy, A. Nahata, M.A. Scarpulla, B. Sensale-Rodriguez, Ultrafast thz modulators with WSe₂ thin films, *Opt. Mater. Express* 9 (2) (2019) 826–836, <https://doi.org/10.1364/OME.9.000826>.
- [52] L. Deng, J. Teng, H. Liu, Q.Y. Wu, J. Tang, X. Zhang, S.A. Maier, K.P. Lim, C.Y. Ngo, S.F. Yoon, S.J. Chua, Direct optical tuning of the terahertz plasmonic response of InSb subwavelength gratings, *Advanced Optical Materials* 1 (2) (2013) 128–132, <https://doi.org/10.1002/adom.201200032>.
- [53] L. Fekete, F. Kadlec, P. Kužel, H. Némec, Ultrafast opto-terahertz photonic crystal modulator, *Opt. Lett.* 32 (6) (2007) 680–682, <https://doi.org/10.1364/OL.32.000680>.
- [54] S.A. Baig, J.L. Boland, D.A. Damry, H.H. Tan, C. Jagadish, H.J. Joyce, M.B. Johnston, An ultrafast switchable terahertz polarization modulator based on III-V semiconductor nanowires, *Nano Lett.* 17 (4) (2017) 2603–2610, <https://doi.org/10.1021/acs.nanolett.7b00401>.
- [55] Y. Gladush, A.A. Mkrtchyan, D.S. Kopylova, A. Ivanenko, B. Nyushkov, S. Kobtsev, A. Kokhanovskiy, A. Khagai, M. Melkumov, M. Burdanova, M. Staniforth, J. Lloyd-Hughes, A.G. Nasibulin, Ionic liquid gated carbon nanotube saturable absorber for switchable pulse generation, *Nano Lett.* 19 (9) (2019) 5836–5843, <https://doi.org/10.1021/acs.nanolett.9b01012>.